JOURNAL OF GEOPHYSICAL RESEARCH, VOL. 115, C04009, doi:10.1029/2009JC005802, 2010



# Extreme wave climate variability in southern Europe using satellite data

Cristina Izaguirre,[1] Fernando J. Mendez,[1] Melisa Menendez,[1] Alberto Luceño,[2] and Inigo J. Losada[1]

Received 14 September 2009; revised 16 November 2009; accepted 19 November 2009; published 7 April 2010.

[1] A time-dependent generalized extreme value (GEV) model for monthly significant wave height maxima from satellite databases is used to model the seasonal and interannual variability of the extreme wave climate throughout southern Europe. In order to avoid a misleading use of the maxima time series, the classical extreme value model has been modified to cope with nonhomogeneous monthly observations. Seasonality is represented using intraannual harmonic functions in the model, while interannual variability is modeled including North Atlantic and Mediterranean regional scale sea level pressure predictors, such as the North Atlantic Oscillation (NAO), the east Atlantic (EA), or the east Atlantic/western Russian (EA/WR) patterns. The results quantify the strong spatial variability detected in the seasonal location and scale GEV parameters. In general, prominent zonal (west–east) and meridional (north–south) gradients of these location and scale parameters reveal the predominance of low-pressure centers located in the NAO region (e.g., a gradient of 4 m for the location parameter and 1.5 units for the scale parameter between north–south is shown in the month of September). The model also quantifies the influence of regional climate patterns on extreme wave climate. Results show a great influence of NAO and EA on the Atlantic basin (e.g., every unit of the monthly NAO index explains 25 cm of the extreme wave height in the Gulf of Biscay and the EA index explains 20 cm) while the negative phases of EA/WR contribute greatly to the western Mediterranean basin.

**Citation:** Izaguirre, C., F. J. Mendez, M. Menendez, A. Luceño, and I. J. Losada (2010), Extreme wave climate variability in southern Europe using satellite data, *J. Geophys. Res.*, *115*, C04009, doi:10.1029/2009JC005802.

## 1. Introduction

[2] The understanding of extreme wave climate is essential, as population and natural coastal ecosystems can be strongly impacted by changes in extremes compared to changes in average climate. From a socioeconomic point of view, a correct characterization of the wave climate is critical in the design and operation of coastal infrastructures. Usually, extreme wave climate analysis only pays attention to the estimation of return period levels of significant wave heights for homogeneous populations; however, there are numerous cases which require a good knowledge of the time-dependent wave climate variability (e.g., offshore industry, selection of ship routing, coastal flooding risk, hydrodynamics in aquatic ecosystems…). Several authors have already presented studies on different variability time scales, such as seasonality [*Menendez et al.*, 2009] or interannual variability [*Woolf et al.*, 2002; *Mendez et al.*, 2006; *Menendez et al.*, 2008] for specific locations. In this paper, we will take advantage of the increasingly important satellite databases [*Panchang et al.*, 1998; *Woolf et al.*, 2003; *Queffeulou*, 2005] to analyze the spatial variability of relevant magnitudes, focusing on the seasonal and interannual variability of extreme significant wave height. Our area of interest is southern Europe, including the Mediterranean Basin and the eastern North Atlantic Ocean (see Figure 1).

[3] The interannual wave height variability has been related to different regional climate patterns [e.g., *Woolf et al.*, 2002; *Lionello and Sanna*, 2005]. The meteorological forcing of extreme wave climate over the North Atlantic can also be characterized by sea level pressure (SLP) anomalies. The anomalies can persist for several consecutive years, reflecting an important part of the interannual and interdecadal climate variability. The interactions between widely separated parts of the ocean and the atmosphere occurring at different time scales are known as teleconnections. Different teleconnection patterns have been established and studied. In particular, the Atlantic ocean-atmosphere system shows several climate oscillation modes, which appear to coexist [*Okumura et al.*, 2001]. Teleconnections for wave climate are usually identified by processing SLP anomaly fields with a principal component analysis (PCA). This provides

[1] Instituto de Hidráulica Ambiental, Universidad de Cantabria, Santander, Spain.
[2] Departamento de Matemática Aplicada y Ciencias de la Computación, Universidad de Cantabria, Santander, Spain.


0148-0227/10/2009JC005802

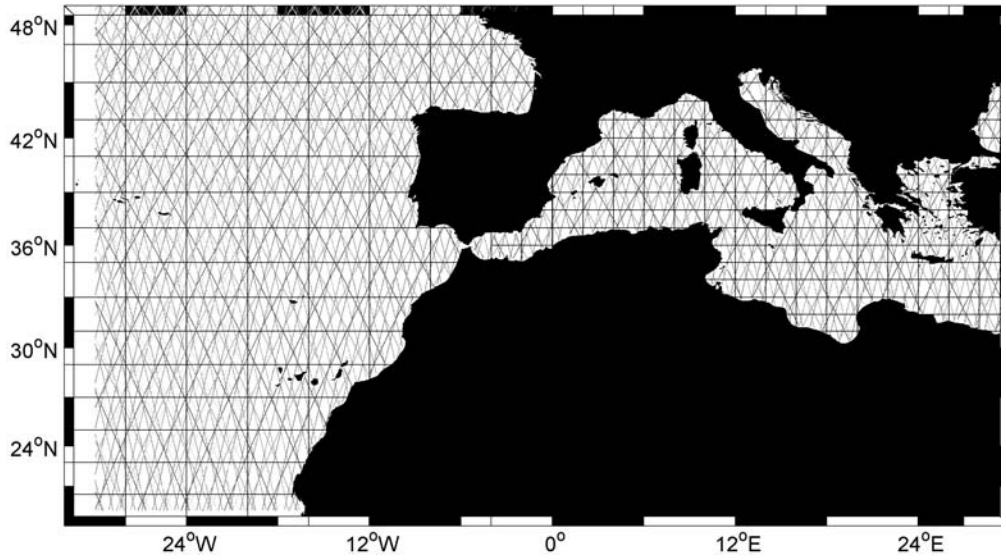


**Figure 1.** Location of the studied area. Rectangular cells used in the analysis are shown (4° × 2° in the Atlantic, 2° × 1° in the Mediterranean). The tracks of the satellite are also displayed.

independent oscillation modes, which are considered to be equivalent to the established teleconnection patterns.

[4] To illustrate the importance of seasonal and interannual variability, the box plot for monthly series maxima is shown in Figure 2 at a particular zone of the study area near the north west coast of Spain. An important modulation in the magnitude and dispersion of monthly maxima is detected (note that the winter season has been placed in the center). The population data time series (gray dots) and monthly maxima (black circles) are shown in Figure 3, where one can see a modulation over time, alternating years of more severe with milder wave climate.

[5] The goal of this paper is to model and quantify the spatial and temporal variability (at intra and inter annual scales) of the extreme significant wave height for an area located in the south of Europe (see Figure 1) by analyzing satellite data. The study area covers from −32° to 30° longitude and from 19° to 49° latitude. The model is based on a time-dependent GEV distribution, using independent monthly maxima events, thus considering 12 maximum values per year [*Menendez et al.*, 2009].

[6] The paper is organized as follows. First, a description of significant wave height and sea level pressure databases is provided. Second, the global framework of the methodology and the statistical model developed is described in section 3. Third, the climatology (on a month-to-month basis) of extreme wave climate is shown. Next, the interannual variability of extreme wave climate in southern Europe is related to atmospheric circulation anomalies in the North Atlantic Oscillation (NAO) area. Finally, some conclusions are given.

## 2. Data Sets

### 2.1. Wave Data

[7] The study of temporal and spatial variability in extreme wave climate requires long-term wave height data covering, with as few and as small as possible spatial or temporal gaps. Since instrumental data is the most reliable information source, satellite data is used in this paper. These have good spatial coverage, although there are some gaps in the time series. Because the number of satellites has increased over time, our time-dependent model must take into consideration the varying number of observations per month.

[8] In this article, we use significant wave height records from five different satellite missions: TOPEX, TOPEX 2, Jason, Envisat, and Geosat Follow-On (GFO). The measurements are taken during different time periods between 1992 and 2006 (see Table 1), which adds a temporal inhomogeneity to the number of data, as can be seen in Figure 4 (all data have been preprocessed). The most severe limitation of satellite altimetry is the scarcity of data, as it takes the

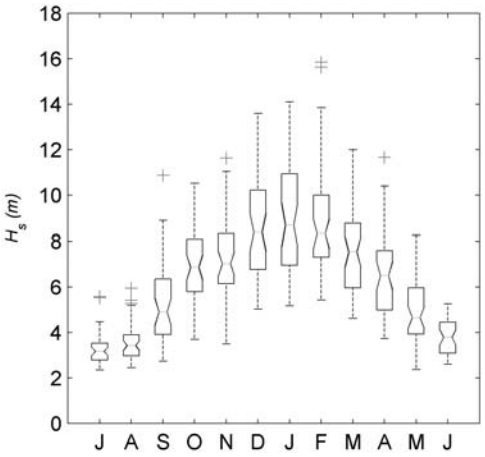


**Figure 2.** Box plots for monthly maxima significant wave height in a particular zone in the studied area. Trapezoidal boxes have lines in the lower, median, and upper quartile values. The whiskers extend to the 1.5 interquartile range or to the range of the data, whichever is shorter, and crosses show outlying values.

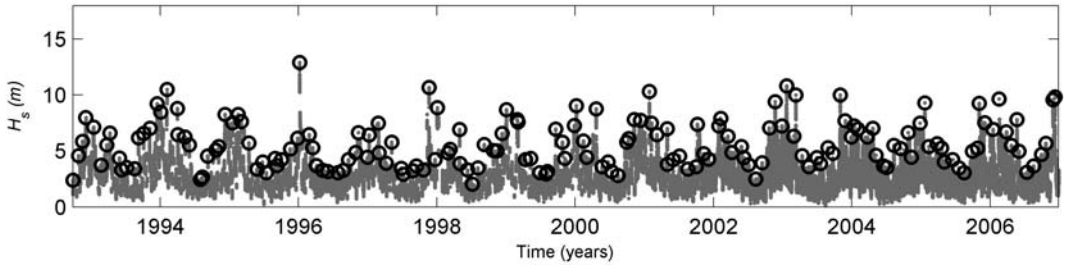


**Figure 3.** Time series of significant wave height (dots) and monthly maxima (circles) in a particular zone in the studied area.

satellite at least 10 days to return to the same point, and only the sea surface directly beneath the satellite is measured.

[9] The study area contains two clearly different basins, the Atlantic and the Mediterranean. After several tests, the Atlantic basin was divided into a 4° × 2° grid (degrees longitude by degrees latitude) seeking a compromise between a representative number of data per cell and the highest spatial resolution. Regarding the Mediterranean basin (with a more pronounced spatial variability due to its complex orography), a 2° × 1° grid has been established giving a greater resolution and ensuring a representative number of data. As an additional step, we have also required that each cell have a minimum number of data. Cells covering part sea and part land can have very few data to obtain realistic monthly maxima. Consequently, we have rejected all cells with less than 30% of $N_{\max}$, where $N_{\max}$ is the maximum number of data per cell ($N_{\max}$ = 119555 for the 4° × 2° cells and $N_{\max}$ = 35014 for the 2° × 1° cells).

### 2.2. Sea Level Pressure Data

[10] The 5° × 5° spatial resolution 6 hourly SLP fields come from the reanalysis data set of the National Centers for Environmental Prediction-National Center for Atmospheric Research (NCEP-NCAR [*Kalnay et al.*, 1996]). We use the eastern North Atlantic (NA) area, which spans from 25° N to 70° N and 60° W to 10° E, covering the North Atlantic storm generation area in southern Europe and which can also be used as a likely teleconnection area for wave climate in the Mediterranean Basin. The reanalysis period used in this study spans from 1958 to 2006.

## 3. Methodology

### 3.1. Summary of the Approach

[11] Studying the influence of seasonal-to-interannual time scales for any geophysical variable $X(t)$ is a statistical challenge. One possibility is to subtract the seasonality, by standardizing the time series $X'(t) = (X(t) - m_i)/\sigma_i$, where $m_i$ and $\sigma_i$ are the mean and standard deviation of the data at a particular $i$th month [*Lionello and Sanna*, 2005]. The standardized variable $X'(t)$ can be later on correlated to any climate-related teleconnection index, such as NAO. By fitting a simple regression model such as $X'(t) = a_{NAO}\mathrm{NAO}(t)$, we can obtain the contribution of parameter $a_{NAO}$ and its statistical significance. Another possibility is to fit a standard regression model to the original time series considering the intraannual variability, such as $X(t) = a_0 + a_1 \cos(\omega t) + a_2 \sin(\omega t) + a_{NAO}\mathrm{NAO}(t)$, where $\omega = 2\pi$ year$^{-1}$ and $t$ is given in years. One important drawback to these methods is that they are modeling the mean of $X(t)$. However, in the context of extreme values of geophysical variables this approach is not valid, as we need to model not only the mean but also the variance and the shape of the distribution. More specifically, we will use the GEV distribution which is defined in terms of a location, a scale and a shape parameter. Therefore, we propose an extension of the regression models to deal with extreme values of a geophysical variable [*Katz et al.*, 2002; *Mendez et al.*, 2006; *Menendez et al.*, 2009]. The first step is to obtain the "seasonality" or the "climatology" of extreme events by fitting a time-dependent GEV model using harmonic functions for the location,

**Table 1.** Measurement Periods of Satellite Missions

| Satellite | Initial Date | Finish Date |
|---|---|---|
| TOPEX 1 | March 1992 | August 2002 |
| TOPEX 2 | September 2002 | October 2005 |
| Jason | January 2002 | December 2006 |
| Envisat | September 2002 | December 2006 |
| GFO | January 2000 | December 2006 |

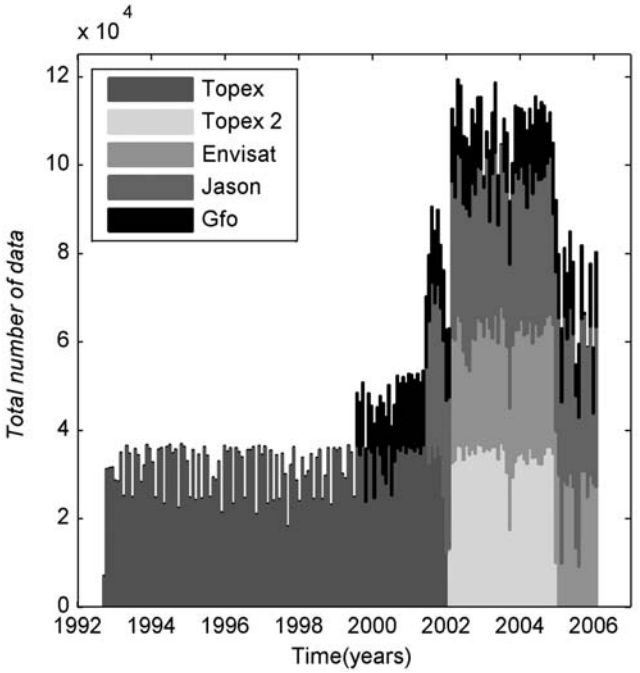


**Figure 4.** Number of measurements per month for each satellite mission.

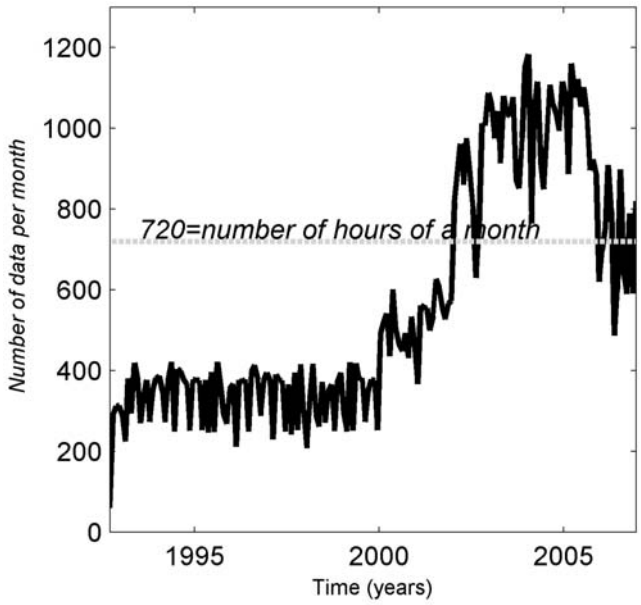


**Figure 5.** Number of satellite data per month for one generic cell.

$\mu(t) = \beta_0 + \beta_1 \cos(\omega t) + \beta_2 \sin(\omega t)$, and scale parameters, $\psi(t) = \alpha_0 + \alpha_1 \cos(\omega t) + \alpha_2 \sin(\omega t)$. Next, the interannual variability is addressed adding an extra contribution to the location parameter. For instance, for the NAO we will propose the following parameterization: $\mu(t) = \beta_0 + \beta_1 \cos(\omega t) + \beta_2 \sin(\omega t) + \beta_{NAO} NAO(t)$. Subsequently, the significance of parameter $\beta_{NAO}$ can be tested using several asymptotically equivalent likelihood tests. In the following paragraphs, we will describe the main characteristics of the developed model.

### 3.2. Time-Dependent GEV Distribution

[12] The generalized extreme value distribution characterizes the classical model on extreme value theory. The model focuses on the statistical behavior of the maxima series

$$\{Z_N = \max(H_1, \ldots, H_N)\}, \tag{1}$$

where ($H_1$, …, $H_N$) is a sequence of sampled significant wave heights. The sequence can, in general, represent any stochastic natural process, based on instantaneous measurements from satellite data, so that $Z_N$ corresponds to the maximum of the process over $N$ observations.

[13] The GEV model usually works with a sample of maxima values $Z_N$ from blocks of equal number of data $N$. For our purposes, we have defined the block span as a month, hereby allowing us to analyze the seasonal and interannual time scales we are interested in. These maxima blocks are often assumed to be independent and identically distributed random variables. However, monthly maxima $Z_t$ of the significant wave heights observed in month $t$ have characteristics that change systematically due to the natural climate variability. Therefore, the hypothesis of homogeneity through consecutive months is not fulfilled (because they are not presumed to be identically distributed).

[14] For that purpose, a nonstationary extreme model is used considering time-dependent location $\mu(t)$, scale $\psi(t) > 0$, and shape $\xi(t)$ parameters of the GEV [*Coles*, 2001]. The cumulative distribution function (CDF) of $Z_t$ is therefore given by

$$F_t(z) = \begin{cases} \exp\left\{-\left[1+\xi(t)\left(\frac{z-\mu(t)}{\psi(t)}\right)\right]_+^{-1/\xi(t)}\right\} & \xi(t) \neq 0 \\ \exp\left\{-\exp\left[-\left(\frac{z-\mu(t)}{\psi(t)}\right)\right]\right\} & \xi(t) = 0 \end{cases}, \tag{2}$$

where $[a]_+ = \max[a, 0]$.

[15] The GEV distribution includes three distribution families corresponding to the three different types of tail behavior: Gumbel family, in the case of a null shape parameter, with a light tail decaying exponentially; Fréchet distribution, with $\xi > 0$ and a heavy tail decaying polinomially; and Weibull family, with $\xi < 0$ and a bounded tail (note that this Weibull for maxima distribution differs from the commonly used Weibull for minima distribution adopted for many other engineering applications).

[16] As mentioned in section 2.1, satellite data records are heterogeneous in the number of data through time due to the addition of different satellite missions. The number of satellite data per month for one generic cell is shown in Figure 5. The different density of data over the years is very relevant (around 300 observations per month during the first 8 years and increasing up to 1000 data per month in later years). Consequently, we must deal with an unequal sample size, which requires adapting the extreme value model to this circumstance.

[17] To solve this problem, a scale factor $k(t) = n(t)/N$ is defined, where $N = 720$ is the usual number of data per month (on a regular hourly time record) and $n(t)$ is the number of satellite observations in month $t$. Assuming that the extreme value distribution for the month with minimum number of observations in satellite data can be adequately represented by a GEV distribution, the modified cumulative distribution function can be written as

$$F_t(z) = \begin{cases} \exp\left\{-k(t)\left[1+\xi^*(t)\left(\frac{z-\mu^*(t)}{\psi^*(t)}\right)\right]_+^{-1/\xi^*(t)}\right\} & \xi^*(t) \neq 0 \\ \exp\left\{-k(t)\exp\left[-\left(\frac{z-\mu^*(t)}{\psi^*(t)}\right)\right]\right\} & \xi^*(t) = 0 \end{cases}, \tag{3}$$

where the GEV parameters are now given by

$$\begin{aligned} &\mu^*(t) = \mu(t) + \frac{\psi(t)}{\xi(t)}\left(k(t)^{\xi(t)} - 1\right), \psi^*(t) = \psi(t)k(t)^{\xi(t)}, \xi^*(t) = \xi(t) && \text{if } \xi^*(t) \neq 0 \\ &\mu^*(t) = \mu(t) + \psi(t)\log k(t), \psi^*(t) = \psi(t), && \text{if } \xi^*(t) = 0 \end{aligned}. \tag{4}$$

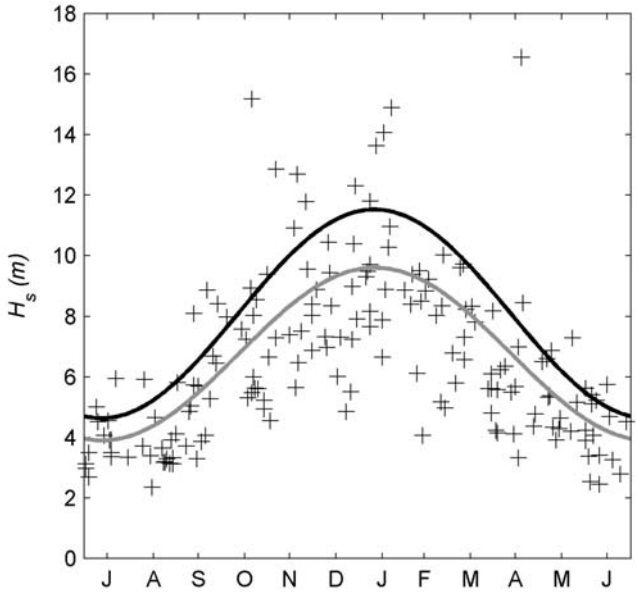


**Figure 6.** Fitted time-dependent location (gray line) and location plus scale parameter (black line) for the data from a cell located in the upper left corner of the domain (30°W, 48°N). Observed values of monthly maxima significant wave height indicated by crosses.

Note that for a regular time scale record we could take $k(t) = 1$, so that equation (3) would be equivalent to (2) and the GEV parameters would remain unchanged.

### 3.3. Regression Model for Seasonality

[18] After a visual inspection of the box plot of Figure 2, it seems reasonable to allow the introduction of harmonic functions to model seasonality [*Menendez et al.*, 2009]. After some tests, we have found that the best common seasonal pattern contains annual cycles for the location and scale parameters, $\mu(t) = \beta_0 + \beta_1 \cos(\omega t) + \beta_2 \sin(\omega t)$ and $\psi(t) = \alpha_0 + \alpha_1 \cos(\omega t) + \alpha_2 \sin(\omega t)$, and a null value for the shape parameter, which implies Gumbel behavior. In this model $\beta_0$ and $\alpha_0$ are mean values; $\beta_i$ and $\alpha_i$ are the amplitudes of the harmonics; $\omega = 2\pi$ year$^{-1}$; and $t$ is given in years. The number of significantly nonnull regression parameters is therefore $p = 6$. The parameters of the representative seasonal model can be packed into the reduced vector $\theta = (\beta_0, \beta_1, \beta_2, \alpha_0, \alpha_1, \alpha_2)$. For $m$ observations of monthly maxima $Z_{ti}$ occurring at instants $t_i$, the model parameters $\hat{\theta}$ are estimated by the maximum likelihood method [*Menendez et al.*, 2009]. An example of the model application for the upper left cell of the study area is shown in Figure 6. Observed values of monthly maxima significant wave heights $Z_{ti}$ are indicated by crosses. The fitted model ($\mu(t) = 6.75 + 2.81\cos(\omega t) + 0.44\sin(\omega t)$, $\psi(t) = 1.32 + 0.59\cos(\omega t) - 0.07\sin(\omega t)$, both parameters in meters), is able to detect a strong modulation in both the location parameter (dashed line) and the location plus the scale parameter (solid line).

### 3.4. Regression Model for Interannual Variability

[19] According to different authors, wave climate in the North Atlantic Ocean and in the Mediterranean basin is related to changes in zonal circulation in the atmosphere [*Woolf et al.*, 2003; *Lionello and Sanna*, 2005]. The atmosphere patterns of pressure anomalies are usually expressed in terms of regional climate index time series. In this work, we have considered two different approaches to quantify the relationship between extreme wave climate and regional climate indices. In the first place, four existing European regional climate patterns were introduced to model interannual variability: NAO, east Atlantic (EA), east Atlantic/western Russian (EA/WR), and Scandinavia pattern (SCA). Each mode has been included by adding a linear term to the location parameter. Mathematically, the model including the influence of NAO can be expressed as

$$\mu(t) = \beta_0 + \beta_1 \cos(\omega t) + \beta_2 \sin(\omega t) + \beta_{NAO} NAO(t), \quad (5)$$

where the parameter $\beta_{NAO}$ represents the influence on extreme wave height per unit of climatic index of NAO in a particular month, $t$. Similar models can be built for the EA, EA/WR, and SCA indices, obtaining $\beta_{EA}$, $\beta_{EA/WR}$, and $\beta_{SCA}$, respectively. Moreover, we have applied a principal component (PC) analysis for the standardized SLP anomalies from the eastern North Atlantic area (see area in section 2.2) to obtain a stronger correlation between these PCs and the anomalies of extreme wave climate. Therefore, similar models have been built for each PC obtaining $\beta_{NA_1}$, $\beta_{NA_2}$, …. Following the example of Figure 6, the fitted model including the influence of NAO leads to $\mu(t) = 6.68 + 2.72\cos(\omega t) + 0.37\sin(\omega t) + 0.41 NAO(t)$, that is, every unit of NAO index explains 0.41 m of positive anomaly of extreme wave climate.

## 4. Climatology of Extreme Wave Climate

### 4.1. Spatial Variability of GEV Parameters

[20] Seasonality explains a great deal of the data variability. We have analyzed the characteristics of the month-to-month variability of storminess using the spatial maps of the location and scale parameters. For a Gumbel distribution, the location parameter $\mu$ coincides with the most probable value of the distribution, and the scale parameter equals $\sqrt{6}/\pi$ times the standard deviation. Therefore, these parameters help us analyze the usual monthly storminess (location parameter) and its average variability or dispersion (scale parameter) for every point. A strong spatial variability is detected in the seasonal location and scale GEV parameters as shown in Figure 7. In general, prominent zonal (west–east) and meridional (north–south) gradients of these location and scale parameters reveal the predominance of low-pressure centers located in the NAO region. In the Mediterranean, the complex spatial pattern of the wavefield is conditioned by regional circulation combined with fetch-limited areas.

### 4.2. Return Levels

[21] A quantile of the wave height probability distribution has been chosen to inform of the extreme wave climate in each particular grid cell. The quantile selected is the 50 year return level annual quantile, $H_{s_{50}}$, corresponding to a given probability of no exceedance $1 - q$ (where the probability of exceedance is $q = 1/50$) and an interval $[t_a, t_b]$ equal to

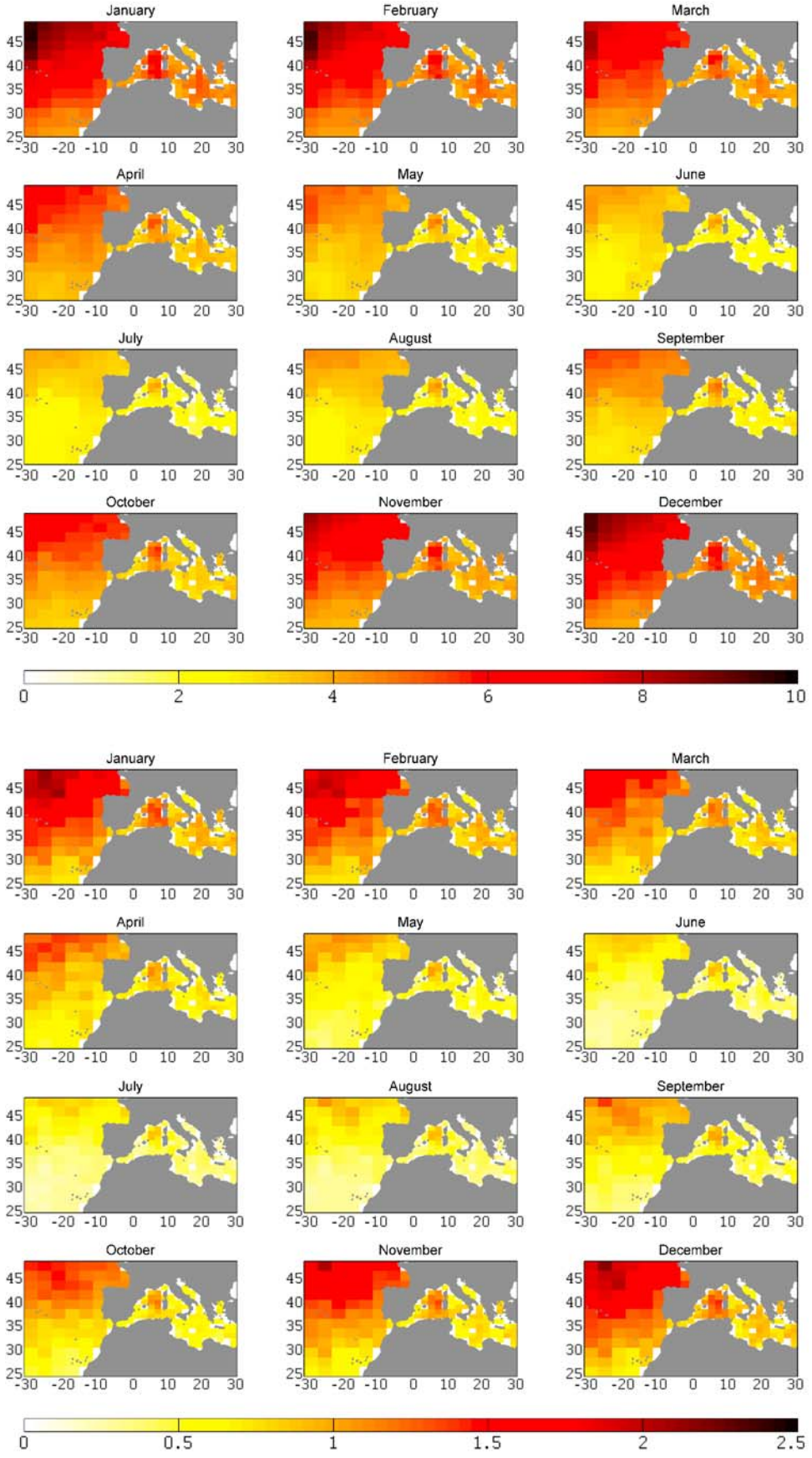


**Figure 7.** Spatial variability on a month-to-month basis of the (top) location (m) and (bottom) scale parameters.

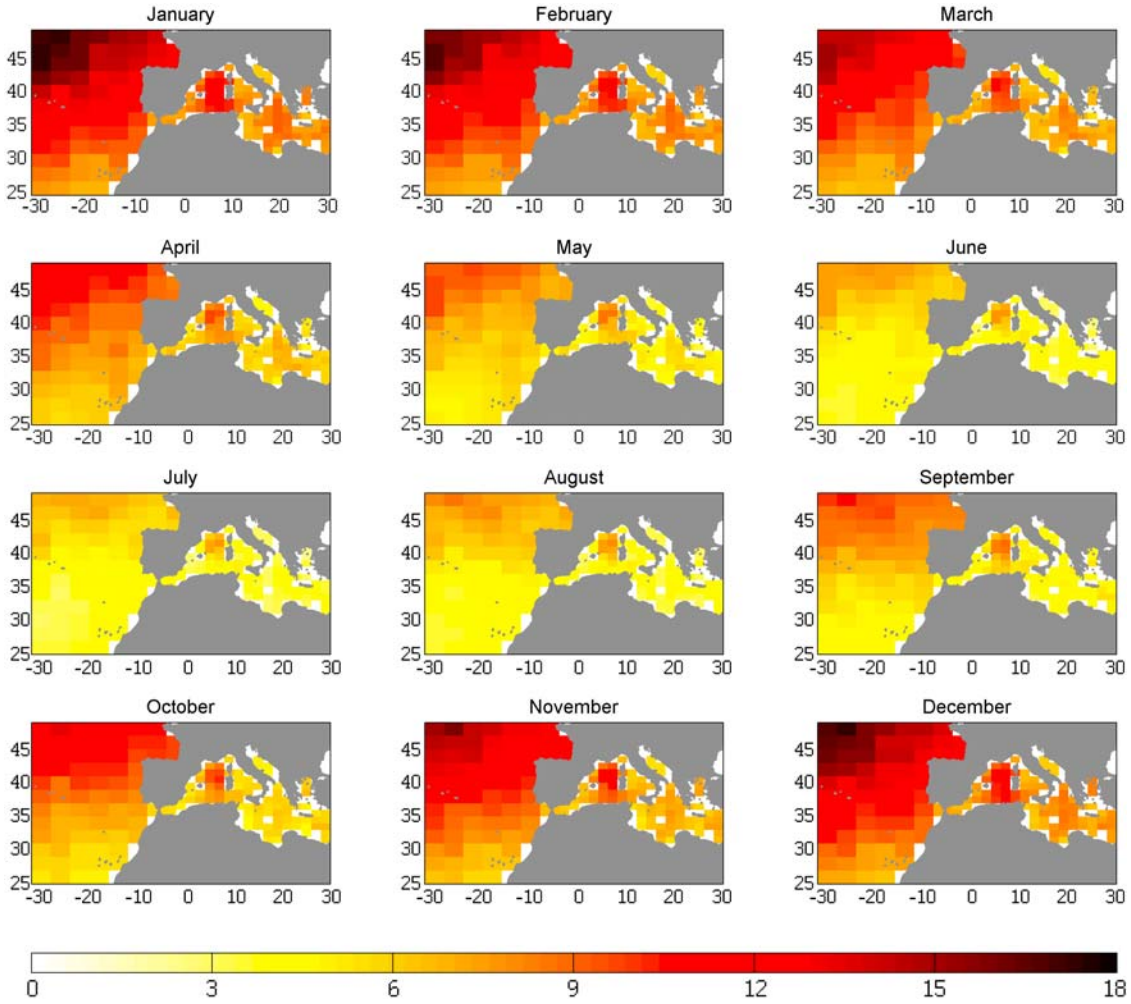


**Figure 8.** Spatial variability of the monthly $H_{s_{50}}$ (m), calculated for each month from the represented seasonal model of the studied area and satellite data.

1 month (e.g., $t_a = (i-1)/12$ and $t_b = i/12$ for a generic month $i$). This can be obtained by iteratively solving

$$1 - q = \exp\left\{ -k_m \int_{t_a}^{t_b} \left[ 1 + \xi^*(t) \left( \frac{\overline{z}_q[t_1, t_2] - \mu^*(t)}{\psi^*(t)} \right) \right]_+^{-1/\xi^*(t)} dt \right\}, \tag{6}$$

where $1/k_m$ is the length of the block maxima, (that is, 1 month, so that $1/k_m = 1/12$ year), and the GEV parameters are given in equation (4).

[22] Figure 8 shows the spatial variability of the monthly $H_{s_{50}}$ along the studied area. As expected, the most severe wave climate takes place during the winter months (November, December, January, February, and March) with maximum values of approximately 18 m in the upper left corner of our analyzed area. These month-to-month results are a very useful tool for several applications, such as the modeling of: coastal community variability, an operability design conditions for maritime works, a probabilistic design of short sea shipping routes, or a design of a device for wave extracting energy.

[23] Looking at the Atlantic basin, the largest wave heights are located in the north western sections, particularly in the Azores Islands and the north and west of the Iberian Peninsula. During winter months, the expected $H_{s_{50}}$ is around 15 m, while in the summer months (June, July, and August) the wave climate is milder, with values of $H_{s_{50}}$ around 5 m. This pattern agrees with the typical northwest storms, causing the most energetic swells for this area.

[24] The Mediterranean basin presents a more moderate wave climate, compared to that of the Atlantic, with maximum $H_{s_{50}}$ close to 10–11 m during winter months. According to satellite data, the largest wave heights are recorded between the Balearic Islands and Corse and Sardinia islands ($H_{s_{50}}$ around 11 m in January, February, or March) and in the Ionian Sea ($H_{s_{50}}$ around 9 m in January, February, or March). For the particular case of the western Mediterranean, the most intense waves are generated by northeastern storms, which introduce northeast winds (known in Spain as *llevantades*) and generate large waves in this part of the basin (e.g., the November 2001 storm produced large swells in the Gulf of Leon [*Ponce de León and Guedes Soares*, 2008]) and also by northwestern storms, associated to very intense *mistral* winds between the

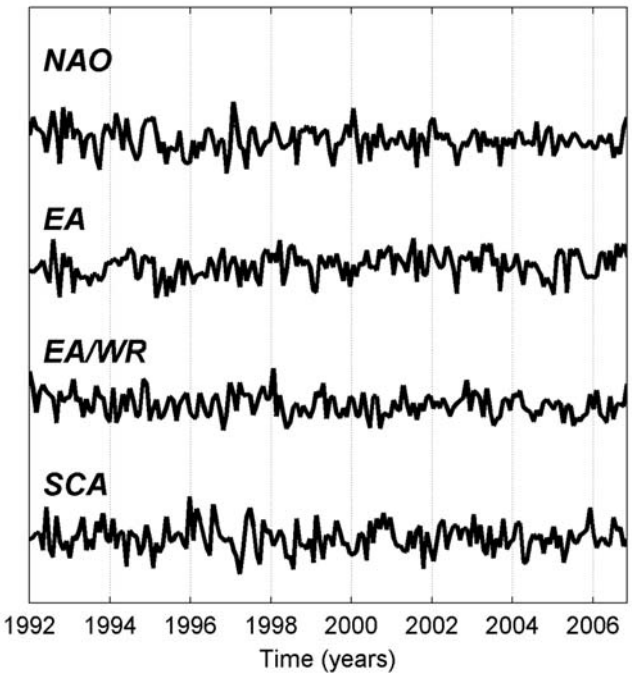


**Figure 9.** Time series of the NAO, EA, EA/WR, and SCA indices.

Balearic Islands and Corse and Sardinia Islands [*Bertotti and Cavaleri*, 2008].

## 5. Interannual Variability of Extreme Wave Climate

### 5.1. Choosing the Predictors

[25] Once the seasonal signal of extreme wave climate is captured, we assume that the anomalies of extreme wave climate with respect to the average (1992–2006) climatology are affected by changes in the zonal circulation of the atmosphere in the extratropical Northern Hemisphere. The relationship between extreme wave climate interannual variability and large-scale atmospheric pressure patterns over the North Atlantic must be explored. To address this problem, two different approaches were considered. In the first place, different existing European regional climate patterns were used to model interannual variability. The second approach consisted of applying a principal component analysis for the standardized SLP anomalies from the eastern North Atlantic area (see area in section 2.2), trying to obtain a stronger correlation between these PCs and the anomalies of extreme wave climate. As mentioned in section 3.4, the study of the influence of teleconnection patterns on the interannual variability of the extreme wave climate has been carried out by adding a new linear term as a predictor to the location parameter following equation (5).

### 5.2. Regional Climate Indices

[26] One of the most prominent teleconnection patterns of all seasons in the North Atlantic basin is the North Atlantic Oscillation [*Barnston and Livezey*, 1987]. The NAO consists of a north–south dipole formed by the Iceland low and the Azores high [*Hurrell*, 1995], producing changes in the mass and pressure fields that modify the paths of the storms crossing the North Atlantic from the east coast of America to Europe. A number of indices have been published that vary according to the sites and instruments. In this work, we have taken the NAO index from *Jones et al.* [1997] which uses data from instruments in Gibraltar and Iceland.

[27] The second prominent mode of low frequency over the North Atlantic basin is the east Atlantic pattern [*Barnston and Livezey*, 1987]. It appears as a leading mode in all months and is structurally similar to the NAO. It consists of a north–south dipole of anomaly centers spanning the North Atlantic from east to west. The anomaly centers of the EA pattern are displaced south–eastward to the approximate nodal lines of the NAO, so that these two modes appear to be interdependent. However, the lower-latitude center contains a strong subtropical link in association with modulations in the subtropical ridge intensity and location. This subtropical link distinguishes the EA pattern from its NAO counterpart. Both NAO and EA modes were found to be significant to explain mean wave height anomalies in the North Atlantic [*Woolf et al.*, 2003].

[28] Two more modes in the extreme wave height are studied in this paper. The east Atlantic/western Russia pattern is one of the three prominent teleconnection patterns that affect Eurasia throughout the year. This pattern is prominent in all months except June–August. This pattern has been referred to as the Eurasia-2 pattern by *Barnston and Livezey* [1987]. It consists of four main anomaly centers. Two main anomaly centers, located over the Caspian Sea and western Russia, comprise the east Atlantic western Russia pattern in winter. A three-celled pattern is therefore evident in the spring and fall seasons, with two main anomaly centers of opposite signs located over western/north western Russia and north western Europe. The third center, having the same sign as the Russian center, is located off the Portuguese coast in spring, but exhibits a pronounced retrogression toward Newfoundland (Canada) in the fall.

[29] Finally, the SCA consists of a primary circulation center that spans Scandinavia and large portions of the Arctic Ocean, north of Siberia. The Scandinavia pattern has been previously referred to as the Eurasia-1 pattern by *Barnston and Livezey* [1987]. Two additional weaker centers with opposite signs to the Scandinavia center are located over western Europe and over the Mongolia/western China sector. This pattern is a prominent mode of low-frequency variability in all months, except June and July. The standardized time series of these four teleconnection patterns for the 1992–2006 period are shown in Figure 9 and the EA, EA/WR, and SCA were obtained from the Website http://www.cpc.noaa.gov/data/teledoc/scand.shtml.

### 5.3. Principal Component Analysis of SLP

[30] We have used spatial and temporal (month-to-month) standardized monthly mean SLP fields, obtaining dimensionless SLP anomaly fields. Monthly SLP anomalies provide information about the severity or roughness of extreme wave climate in that particular month. This contribution has been included in the model as the location parameter of the GEV distribution. A principal component analysis has been applied to the SLP anomaly fields. The central idea of PCA,

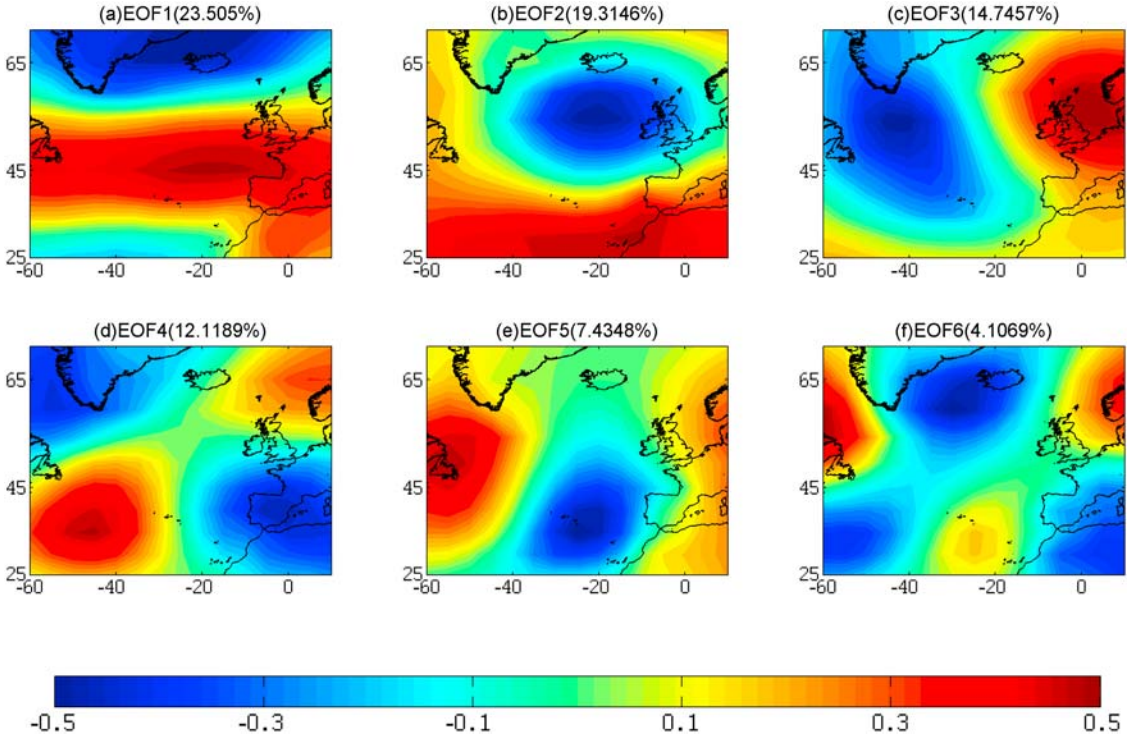


**Figure 10.** EOFs of the sea level pressure anomalies in the North Atlantic area. Numbers in brackets represent the explained percent variance for each mode.

or empirical orthogonal functions (EOFs) approach as it is also known as in the meteorological literature, is to reduce the dimensionality of a data set consisting of a large number of interrelated variables, while retaining as much variation in the data set as possible. This is achieved by transforming the original set of variables into a new data set, the principal

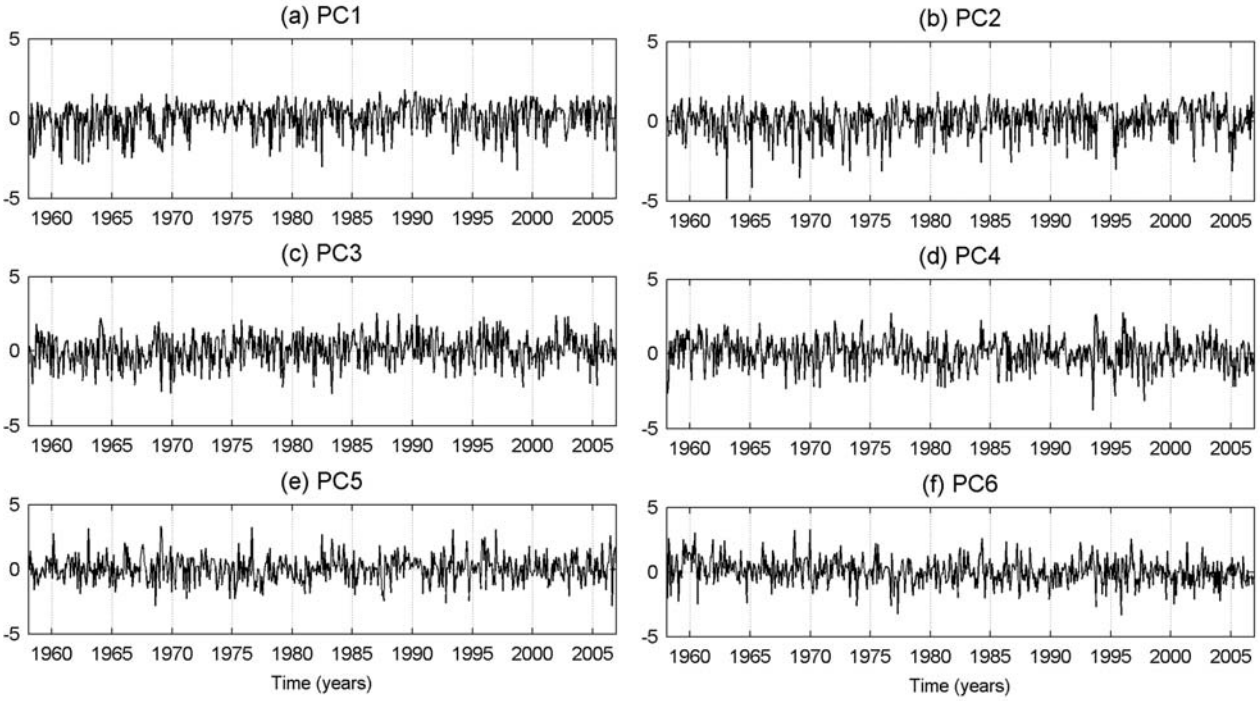


**Figure 11.** Standardized PCs of the sea level pressure anomalies in the North Atlantic area.

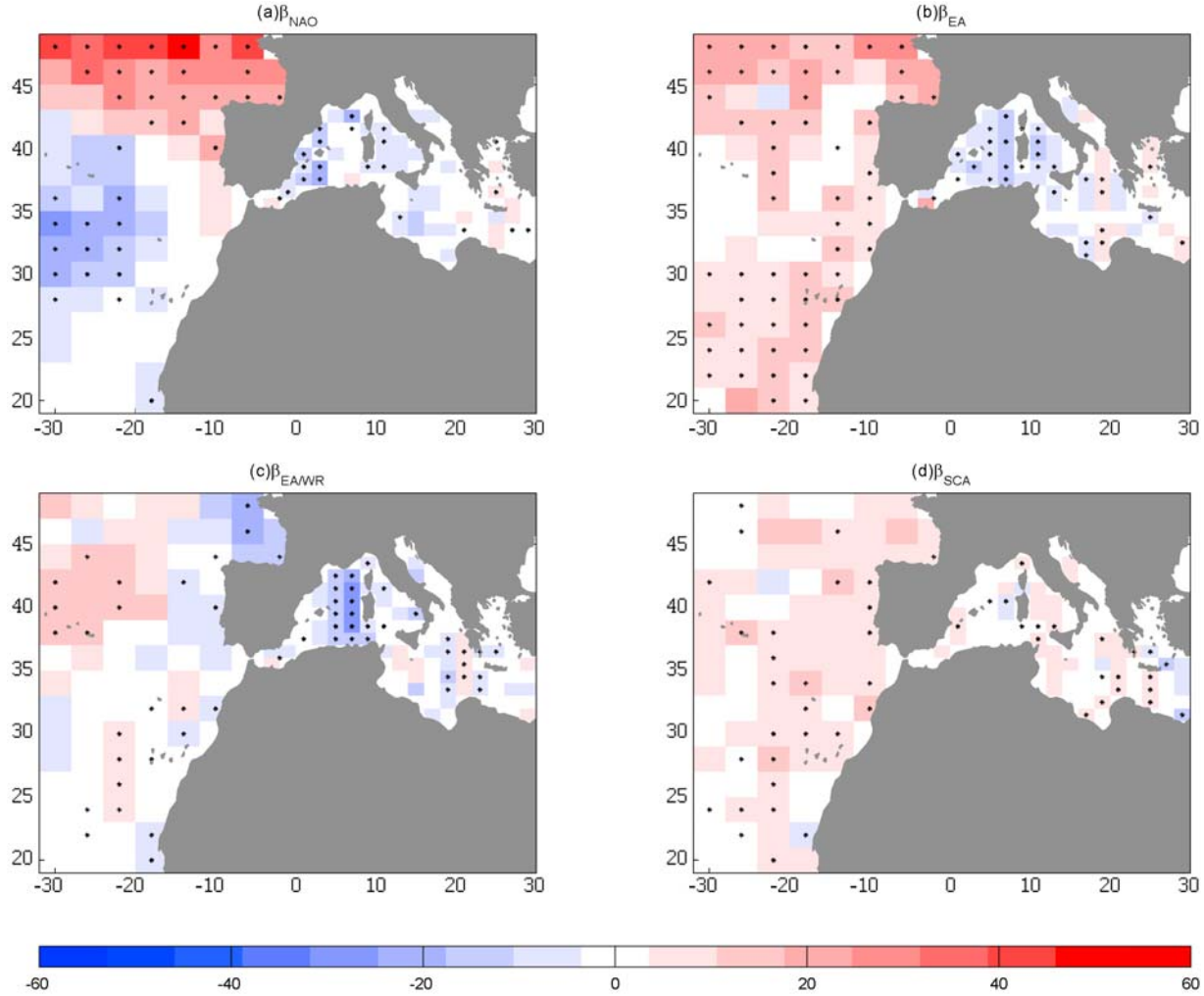


**Figure 12.** Spatial variability of the influence of the climate indices on the location parameter: (a) $\beta_{NAO}$, (b) $\beta_{EA}$, (c) $\beta_{EAWR}$, and (d) $\beta_{SCA}$ (cm/unit). Statistical significance level smaller than 10% is represented by an asterisk in the middle of the cell.

components. These are mutually uncorrelated and can be in decreasing order of explained variability. The analysis of the SLP anomalies yields the spatial modes and their corresponding temporal amplitudes. We retain the modes that explain more than 4% of the data variability ($M$ = 6 modes for the North Atlantic area). Figure 10 shows the first 6 EOF maps of the North Atlantic area, while Figure 11 shows the associated PC time series. As expected, the first PC of NA area is highly correlated with NAO ($r$ = 0.68), while the second PC is more correlated with EA pattern ($r$ = 0.63) than with NAO ($r$ = 0.42).

### 5.4. Spatial Variability of Extreme Wave Climate Interannual Variability

[31] Figure 12 shows the spatial variability of the influence of the NAO, EA, EA/WR, and SCA standardized indices ($\beta_{NAO}$, $\beta_{EA}$, $\beta_{EAWR}$, $\beta_{SCA}$, respectively) on the location parameter. The statistical significance at a 10% level of each climate index is shown in the center of each cell with an asterisk. According to Figure 12, the most influential pattern in the studied area corresponds to NAO, EA, and EA/WR indices (every unit of standardized index explains a certain magnitude of significant wave height). The parameter $\beta_{NAO}$ has a clear spatial pattern and heavy influence in the Azores area and is also significant, although less intense, in the Mediterranean basin. The parameter $\beta_{EA}$ also has a clear spatial pattern with a significant and strong influence in the Atlantic basin. Finally, $\beta_{EAWR}$ shows an important influence on the Mediterranean basin, especially between the Balearic Islands and Corse and Sardinia Islands.

[32] A relationship between the NAO index and northwest storms, which causes the typical swells formed in the North Atlantic basin, is detected in Figure 12a. Therefore, years with an intense positive phase of NAO have greater northwest swells, due to the important contribution of NAO pattern. One advantage of this model is that we are able to quantify the influence of these teleconnective indices in the intensity of the extremes. For instance, every unit of NAO index explains 20 cm of the extreme wave height in the Bay of Biscay. Looking at a specific instant, e.g., February 1997,

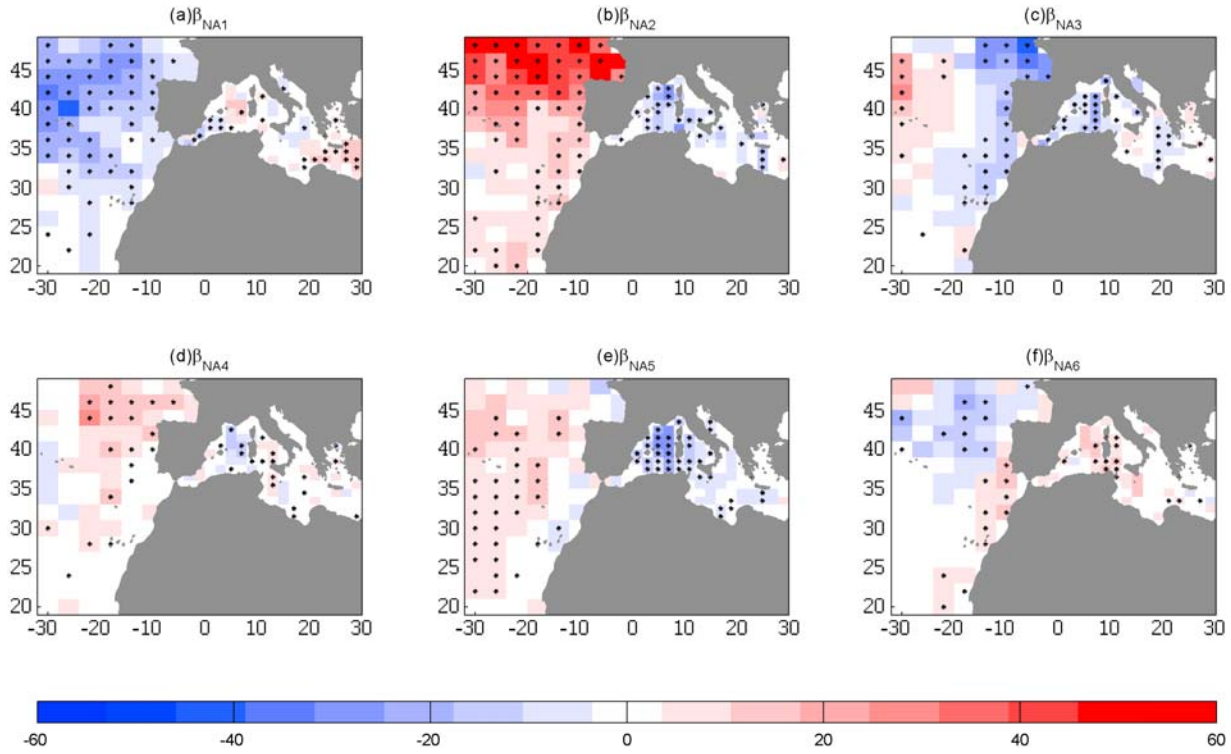


**Figure 13.** Spatial variability of the influence of the PCs of the sea level pressure anomalies in the NA area on the location parameter: (a) $\beta_{N_{A1}}$, (b) $\beta_{NA_2}$, (c) $\beta_{NA_3}$, (d) $\beta_{NA_4}$, (e) $\beta_{NA_5}$, and (f) $\beta_{NA_6}$ (cm/unit PC). Statistical significance level smaller than 10% is represented by an asterisk in the middle of the cell.

the NAO index was 5.2, therefore 1.04 m of wave height (5.2 units × 20 cm/unit = 104 cm) was due to the influence of this climatic index. Using the leading information of the NAO index, the model can be used to predict the probability of exceedance of a given extreme wave height in each location of the studied area, including the seasonality and the interannual variability. In the western Mediterranean, negative phases of the NAO pattern produce positive anomalies in extreme significant wave heights.

[33] Figure 12b shows the influence of the EA pattern on the extreme wave height. One can see a clear match with the synoptic EA situation, with positive influence in the Atlantic basin. We can conclude that positive phases of the EA index produce a good contribution to northwest swells, as in the case of NAO. In the Mediterranean, a smaller and more spread out contribution to the extreme wave height for the negative phases of the EA pattern between the Spanish and Italian coasts is detected.

[34] Figure 12c shows a large influence of the negative phases of the EA/WR pattern between the Balearic Islands and the islands of Corse and Sardinia, in the Mediterranean basin. According to it, negative phases of the EA/WR index might affect the northeast swells in the Mediterranean, increasing extreme wave height in this area. For example, in October 1987 the EA/WR index was −2.73 units, hence 54.6 cm of wave height in the area between Balearic and Corse and Sardinia Islands is due to this teleconnection.

[35] Finally, results for the SCA index can be observed in Figure 12d. It shows a homogeneous and slightly positive pattern along the eastern part of the Atlantic area for positive phases of the SCA index although with a very low intensity (the most significant area is around the Canary Islands, where every unit of SCA index explains 15 cm of wave height).

[36] The influence of the first 6 PCs of NA area is shown in Figure 13. Figures 13a and 13b show very similar patterns with the two prominent teleconnections in the North Atlantic, NAO and EA, (see correlations between PCs and climate indices in Table 2) but with a more intense contribution. A clear pattern of positive influence with negative phases of $PC_1$ and positive phases of $PC_2$ appears in the upper part of the Atlantic basin in the studied area. For instance, every positive unit of the standardized $PC_{NA2}$ contributes 50 cm to the extreme wave height in the Bay of Biscay. Figure 13c shows the influence of $PC_3$ in the extreme wave height. One can see that negative phases of the standardized $PC_3$ produce a positive influence (increase in the extreme wave height) around the coast of the Iberian Peninsula. The EOF3 in Figure 10 shows the monthly average climatic situation producing it. A low-pressure

**Table 2.** Correlation Between PCs and NAO and EA

| | NAO | EA | EA/WR | SCA |
|---|---|---|---|---|
| $PC_1$ | 0,676 | 0,072 | 0.035 | 0.165 |
| $PC_2$ | 0,422 | 0,629 | 0.055 | 0.083 |
| $PC_3$ | 0,020 | 0,012 | 0.422 | 0.063 |
| $PC_4$ | 0,281 | 0,145 | 0.030 | 0.464 |
| $PC_5$ | 0,045 | 0,223 | 0.089 | 0.074 |
| $PC_6$ | 0,082 | 0,120 | 0.049 | 0.280 |

center located over the North Sea produces northern winds which contribute to an increase of extreme wave height in the Bay of Biscay.

[37] In the Mediterranean basin, the first two modes (Figures 13a and 13b) have a slightly negative influence similar to that which occurs with the NAO and EA patterns in the western Mediterranean. Mode $PC_1$ also contributes to an increase of the extreme wave height in the eastern Mediterranean. Figure 13c shows a significant contribution to the extreme wave height for negative phases of the $PC_3$ between Balearic and Corse and Sardinia Islands, an area which accounts for the largest waves of the Mediterranean. Figure 13e shows a clear negative influence in the western part of the Mediterranean basin, contributing, in negative phases of the $PC_5$ to an increase in the highest waves in northwestern Africa, over the Maghreb. These anomalies might also be explained with the western Mediterranean Oscillation, WEMO [*Martin-Vide and López-Bustins*, 2006], as the correlation between WEMO and the third and fifth PCs are $r = 0.4$ and $r = 0.31$, respectively. The maximum contribution is 40 cm per negative unit of $PC_5$ between Balearic and Corse and Sardinia Islands, where the highest waves of the Mediterranean are expected.

## 6. Conclusions

[38] The seasonal-to-interannual and spatial variability of extreme wave climate in southern Europe-eastern North Atlantic and the Mediterranean Sea is analyzed using a statistical model based on the time-dependent generalized extreme value distribution for independent monthly maxima series of significant wave heights [*Menendez et al.*, 2009] able to deal with the unequal sample size of satellite data. Seasonality is introduced in the GEV distribution using harmonic functions that represent the annual cycle through the location and scale parameters of the GEV distribution of extreme significant wave height. Interannual variability is introduced via the location parameter as linear covariates in two different ways. First, using known climate related regional indices such as the NAO, EA, EA/WR, and SCA and, second, by means of PCs of monthly SLP anomalies in the North Atlantic and Mediterranean Basin.

[39] The climatology of extreme wave climate in the eastern North Atlantic, on a month-to-month basis, reveals a strong north-to-south gradient according to the predominance of low-pressure centers located in the NAO region. In the Mediterranean, local circulation and fetch-limited areas produce a complex spatial pattern. The most energetic area is located between the Balearic Islands and Corse and Sardinia Islands and is associated to *mistral* and *llevantade* winds that generate NW and NE severe storms, respectively, which agrees with the studies of *Ponce de León and Guedes Soares* [2008] and *Bertotti and Cavaleri* [2008]. High return-level values, such as the month-to-month 50 year return level of significant wave height, can be used for various applications: to determine the survivability of coastal communities, for the operability design of specific maritime works and for the design of ship routes or wave energy farms.

[40] Moreover, the interannual variability analysis reveals that NAO and EA indices seem to be the most influential patterns in the North Atlantic area. Positive phases of the NAO index have a large positive influence on the extreme wave climate of the Bay of Biscay, while positive phases of the EA pattern show a general increase of severity in the studied Atlantic region and a decrease in the western Mediterranean basin. Negative phases of EA/WR pattern contribute to increase the storminess in the western Mediterranean basin, influencing the swells from northeast storms. Results for the PCs of SLP anomalies enhance these findings: first two PCs of the NA have similar patterns of influence to NAO and EA indices. The rest of the PCs show local variability in the storminess linked to regional cyclone activity.

[41] **Acknowledgments.** The work was partially funded by projects "GRACCIE" (CSD2007–00067, CONSOLIDER-INGENIO 2010) from the Spanish Ministry of Ciencia e Innovación, "MARUCA" from the Spanish Ministry of Fomento and "C3E" from the Spanish Ministry of Environment, Rural and Marine Affairs. Alberto Luceño acknowledges the support of the Spanish Dirección General de Investigación under grant MTM2008–00759. The authors wish to thank the two anonymous reviewers for their constructive comments that helped to improve the manuscript.

## References

Barnston, A. G., and R. E. Livezey (1987), Classification, seasonality and persistence of low-frequency atmospheric circulation patterns, *Mon. Weather Rev.*, *115*, 1083–1126, doi:10.1175/1520-0493(1987)115<1083:CSAPOL>2.0.CO;2.

Bertotti, L., and L. Cavaleri (2008), Analysis of the Voyager storm, *Ocean Eng.*, *35*, 1–5, doi:10.1016/j.oceaneng.2007.05.008.

Coles, S. G. (2001), *An Introduction to Statistical Modelling of Extreme Values*, 208 pp., Springer, London.

Hurrell, J. W. (1995), Decadal trends in the North Atlantic Oscillation: Regional temperatures and precipitation, *Science*, *269*, 676–679, doi:10.1126/science.269.5224.676.

Jones, P. D., T. Jónsson, and D. Wheeler (1997), Extension to the North Atlantic Oscillation using early instrumental pressure observations from Gibraltar and south–west Iceland, *Int. J. Climatol.*, *17*, 1433–1450, doi:10.1002/(SICI)1097-0088(19971115)17:13<1433::AID-JOC203>3.0.CO;2-P.

Kalnay, E., et al. (1996), The NCEP/NCAR 40-year reanalysis project, *Bull. Am. Meteorol. Soc.*, *77*, 437–471, doi:10.1175/1520-0477(1996)077<0437:TNYRP>2.0.CO;2.

Katz, R.W., M. B. Parlange, and P. Naveau (2002), Statistics of extremes in hydrology, *Adv. Water Resour.*, *25*, 1287–1304.

Lionello, P., and A. Sanna (2005), Mediterranean wave climate variability and its link with NAO and Indian Monsoon, *Clim. Dyn.*, *25*, 611–623, doi:10.1007/s00382-005-0025-4.

Martín-Vide, J., and J. A. López-Bustins (2006), The western Mediterranean Oscillation and Iberian peninsula rainfall, *Int. J. Climatol.*, *26* (11), 1455–1475, doi:10.1002/joc.1388.

Mendez, F. J., M. Menendez, A. Luceño, and I. J. Losada (2006), Estimation of the long-term variability of extreme significant wave height using a time-dependent POT model, *J. Geophys. Res.*, *111*, C07024, doi:10.1029/2005JC003344.

Menendez, M., F. J. Mendez, I. J. Losada, and N. E. Graham (2008), Variability of extreme wave heights in the northeast Pacific Ocean based on buoy measurements, *Geophys. Res. Lett.*, *35*, L22607, doi:10.1029/2008GL035394.

Menendez, M., F. J. Mendez, C. Izaguirre, A. Luceño, and I. J. Losada (2009), The influence of seasonality on estimating return values of significant wave height, *Coastal Eng.*, *56*(3), 211–219, doi:10.1016j/coastaleng.2008.07.004.

Okumura, Y., S. Xie, A. Numaguti, and Y. Tanimoto (2001), Tropical Atlantic air-sea interaction and its influence on the NAO, *Geophys. Res. Lett.*, *28*(8), 1507–1510, doi:10.1029/2000GL012565.

Panchang, V., L. Zhao, and Z. Demirbilek (1998), Estimation of extreme wave heights using GEOSAT measurements, *Ocean Eng.*, *26*, 205–225, doi:10.1016/S0029-8018(97)10026-9.

Ponce de León, S., and C. Guedes Soares (2008), Sensitivity of wave model predictions to wind fields in the western Mediterranean Sea, *Coastal Eng.*, *55*(11), 920–929, doi:10.1016/j.coastaleng.2008.02.023.

Queffeulou, P. (2005), Wave height variability over the Mediterranean Sea, using altimeter data, paper presented at 5th International Symposium on Ocean Wave Measurements and Analysis, Coasts, Oceans, Ports and Rivers Inst., Madrid.

Woolf, D. K., P. G. Challenor, and P. D. Cotton (2002), Variability and predictability of the North Atlantic wave climate, *J. Geophys. Res.*, *107*(C10), 3145, doi:10.1029/2001JC001124.

Woolf, D. K., P. D. Cotton, and P. G. Challenor (2003), Measurements of the offshore wave climate around the British Isles by satellite altimeter, *Philos. Trans. R. Soc. London Ser. A*, *361*, 27–31, doi:10.1098/rsta.2002.1103.

C. Izaguirre, I. J. Losada, F. J. Mendez, and M. Menendez, Instituto de Hidráulica Ambiental, Universidad de Cantabria, E.T.S.I. Caminos Canales y Puertos, Av. de los Castros s/n, E-39005 Santander, Spain. (cristina.izaguirre@unican.es; mendezf@unican.es)

A. Luceño, Departamento de Matemática Aplicada y Ciencias de la Computación, Universidad de Cantabria, E.T.S.I. Industriales y de Telecomunicación, Av. de los Castros s/n, E-39005 Santander, Spain.